Probing Excited-State Electron Transfer by Resonance Stark Spectroscopy. 2. Theory and Application

Huilin Zhou and Steven G. Boxer*

Department of Chemistry, Stanford University, Stanford, California 94305-5080

Received: April 28, 1998; In Final Form: August 28, 1998

A theory of the resonance Stark effect data reported in part 1 (preceding paper in this issue) is developed. The model used involves a weak charge resonance interaction between the excited state of an electron donor *D and a vibronically broad charge-separated state D^+A^-, where A is an electron acceptor. The theory predicts a series of unusual higher order Stark line shapes depending primarily on the driving force for electron transfer. These line shapes closely resemble the series of line shapes reported in part 1 for the B_L absorption band of several reaction center variants. Analysis of the trends leads to the conclusion that the novel Stark line shapes are due to coupling between the ^1B_L and $B_L{}^+H_L{}^-$ states. Analysis of the higher order Stark data gives information on the driving force and rates for the $^1B_L \rightarrow B_L{}^+H_L{}^-$ electron-transfer reaction in this series of variants. The rate of this reaction in wild-type reaction centers is about 1 order of magnitude slower than energy transfer from ^1B_L to the special pair as the driving force is quite small; however, it becomes much faster when the driving force is larger, as in the (M)Y210F mutant. Quantitative information is extracted on the rates, relative driving force, and electronic coupling for this process. These results have implications for the mechanism of the primary charge-separation reaction (one-step vs two-step electron transfer) and the origins of unidirectional electron transfer. The experimental method and method of analysis should be generally applicable to any excited-state electron-transfer reaction.

Photoinduced electron-transfer reactions in donor−acceptor (DA) systems are typically studied by time-resolved kinetic measurements. An interesting and common situation is that the D^+A^- state is energetically close to a locally excited or molecular exciton state such as *D. In this situation, a charge resonance interaction between the *D and D^+A^- states can affect the physical nature of *D, and, depending on the strength of this interaction, this can be reflected in the line shape of the absorption spectrum.[1] We recently introduced an approach for analyzing absorption spectra where coupling to *intra*molecular charge-transfer states is important and applied this method to the electronic absorption line shapes of the heterodimer special pair in bacterial photosynthetic reaction centers (RCs).[1] Within a one-electron resonance approximation, it was shown that such charge resonance interactions can affect absorption line shapes as the result of a competition between the charge resonance strength and the electron−phonon coupling associated with charge transfer. In the intermediate coupling limit, large changes in absorption spectral line shapes are expected which can then be used to calculate the excited-state charge resonance nature of a DA complex, and this was used to analyze the electronic absorption spectra of heterodimer special pair variants.[2] In the weak charge resonance limit, however, inhomogeneous broadening typically overwhelms the homogeneous broadening due to the charge resonance interaction, and the absorption spectrum alone does not provide much information on the excited-state charge-transfer dynamics. Nonetheless, the physical nature of this excited state *is* modified by a weak charge resonance interaction, and the methods described here are an approach to uncover these interactions.

In part 1 (preceding paper in this issue), we reported the higher order Stark (HOS) spectra of photosynthetic RCs.[3] A new class of line shapes was observed associated exclusively with the monomeric bacteriochlorophyll (BChl) on the functional side (B_L, see Figure 1, part 1, for a diagram of the RC and notation). The shape and amplitude of this new feature were observed to depend most directly on the nature of the electron

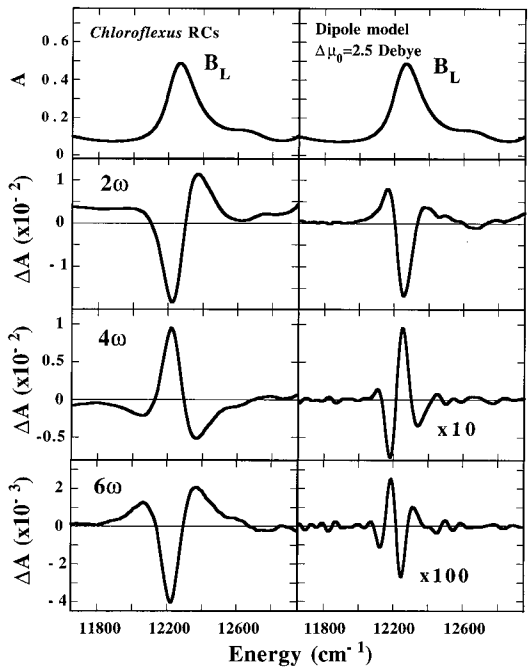

Figure 1. Comparison between the experimental B_L band higher order Stark effects in *Chloroflexus aurantiacus* RCs (left panels) and calculated Stark effects (right panels) that would be predicted using the difference dipole of 2.5 D appropriate for a monomeric bacteriochlorophyll molecule in an organic glass.[4] In both cases, a monomeric bacteriochlorophyll is being observed, but it is evident that the results for RCs require a different mechanism.

10.1021/jp982044o CCC: $15.00
Published on Web 10/21/1998

acceptor in the H_L binding site and on environmental perturbations around B_L, suggesting that the effect may involve some interaction between the ^1B_L state and a charge-separated state such as $B_L^+H_L^-$ or $B_L^-H_L^+$. A striking example summarizing these results is presented in Figure 1, where this novel signal from *Chloroflexus aurantiacus* (*C. aurantiacus*) RC is compared with the signal that would be obtained if the difference dipole moment were that measured for an isolated BChl. This is a particularly good comparison as there is only one BChl (B_L) in this RC, simplifying the spectrum. The calculated spectra shown on the right are what would be expected if the BChl in the RC were behaving as an isolated chromophore; exactly such spectra are obtained for isolated, pure BChl in an organic glass.[4] The signals from the RC have amplitudes that are several orders of magnitude greater than that for an isolated BChl, and their line shapes are completely different; so some new interaction must be present in the RC. In part 1 we showed that a rather large range of line shapes and amplitudes can be obtained for different RCs, so any treatment of this problem must deal with the origin of these variations as well.

With these data and the general issues described above for DA systems as a motivation, we consider in the following the effects of a weak charge resonance interaction between a locally excited state and a charge-separated state on the line shapes observed in higher order Stark measurements. We find that, with reasonable assumptions, Stark line shapes that are drastically different from those predicted by the conventional analysis of Stark data (due largely to Liptay[5]) are expected and that these line shapes resemble what was observed in part 1 for RCs in the B band region. The analysis is used to provide semiquantitative insights into interactions between ^1B_L and $B_L^+H_L^-$, which we will argue are responsible for the unusual Stark effects in RCs. We stress that this treatment should apply to any DA system where relatively weak excited-state charge resonance interaction is present.

Theory

Physical Model and Assumptions. Following the earlier theoretical treatment of charge resonance effects on electronic absorption line shapes,[1] we consider three electronic states in the zero order picture: a ground state, a molecular exciton state, and an intermolecular charge-transfer (CT) state. The electronic coupling term between the exciton and CT states is defined as V_0. Any interaction between the ground and CT states is neglected as these states are very different in energy. It is also assumed that the electronic transition from the ground state to the exciton state is allowed with a transition energy ν_0, while a direct electronic transition from the ground state to the CT state is forbidden in the zero order picture. The vibronic overlap function $G_2(\nu)$ between the exciton and CT states is assumed to be a Gaussian given as

$$G_2(\nu) = \frac{2}{\Delta_{CT}}\left[\frac{\ln 2}{\pi}\right]^{1/2} \exp\left[-4 \ln 2\left(\frac{\nu - \nu_{CT}}{\Delta_{CT}}\right)^2\right] \qquad (1)$$

where Δ_{CT} is the full width at half-maximum (fwhm) of $G_2(\nu)$ and ν_{CT} is the location of its maximum. The absorption line shape in this charge resonance picture is[1]

$$\epsilon_2(\nu) = \frac{|V_0|^2 G_2(\nu)}{[\nu - \nu_0 - |V_0|^2 G_1(\nu)]^2 + \pi^2 |V_0|^4 G_2(\nu)^2} \qquad (2)$$

where $G_1(\nu)$ is the Hilbert transform of $G_2(\nu)$. In the weak charge resonance limit, $\epsilon_2(\nu)$ has an *approximate* Lorentzian line shape whose line width $\pi|V_0|^2 G_2(\nu)$ at $\nu = \nu_0$ is related to the lifetime broadening of the exciton state due to charge transfer by Fermi's Golden rule. The $|V_0|^2 G_1(\nu)$ term at $\nu = \nu_0$ is a resonance energy shift which determines the absorption peak location. The square of the transition dipole moment or oscillator strength is omitted in eq 2, so a multiplicative constant involving the oscillator strength and sample concentration is needed for comparison with any experimental absorption spectrum. The same constant is used for all the higher order Stark spectra whenever a comparison is attempted. A schematic illustration of this charge resonance effect in the weak charge resonance limit is shown in Figure 2.

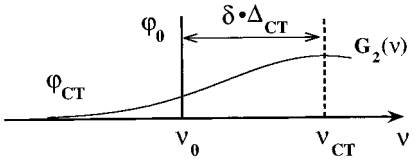

Figure 2. Schematic diagram of the charge resonance interaction between a molecular exciton *D state φ_0 and charge-transfer D^+A^- state φ_{CT}. The transition to the φ_0 state is discrete with frequency ν_0; the vibronic density of states of the CT state is represented by a Gaussian $G_2(\nu)$ with width Δ_{CT} and peak location ν_{CT}. The difference between ν_0 and ν_{CT} is defined as $\delta \cdot \Delta_{CT}$.

To calculate Stark line shapes, it is convenient to recast eq 2 into a form in terms of the complex dielectric function $\epsilon(\nu)$:

$$\epsilon(\nu) = \frac{1}{\nu - \nu_0 - |V_0|^2 G(\nu) - i\Gamma_0} \qquad (3)$$

where the complex dielectric function for the CT state is defined as $G(\nu) = G_1(\nu) + i\pi G_2(\nu)$. Γ_0 is a phenomenological broadening term. If Γ_0 is zero, the imaginary part of eq 3 yields the absorption line shape in eq 2 directly. The experimental absorption spectrum often consists of other broadening mechanisms, such as inhomogeneous broadening or homogeneous broadening due to energy transfer, etc. It is assumed that these broadening mechanisms are not affected by an applied electric field. Because such broadening mechanisms should broaden the calculated Stark effects (due to electric field perturbation of the $|V_0|^2 G(\nu)$ term) in an identical manner as they broaden the absorption spectrum, it is valid and convenient to use eq 3 for subsequent analysis of Stark effects. The absorption spectrum is given by the imaginary part of eq 3, i.e., a Lorentzian line shape.

We now consider the effect of an applied electric field or Stark effect on the dielectric function $\epsilon(\nu)$. We shall assume that electric field effects on the V_0 term can be neglected. Two likely mechanisms for the Stark effect are evident from eq 3. First, the applied electric field will affect the transition energy ν_0 if there is a nonzero intrinsic difference dipole moment $\Delta\mu_0$ between the ground and molecular exciton states in the absence of any intermolecular charge resonance effect. The Stark effect from a nonvanishing dipole $\Delta\mu_0$ will be called a Liptay-type Stark effect because the analysis method originally developed by Liptay is widely used.[4-6] Higher order Stark spectroscopy based on this conventional model was described in part 1 (Experimental Methods) and elsewhere.[4,7] Second, the applied electric field will affect the complex dielectric function $G(\nu)$ of the CT state and consequently affect the charge resonance interaction between the exciton state and CT state. The dielectric function $\epsilon(\nu)$ for the final state, an admixture of the exciton state and CT state, is therefore affected. The Stark effect from this new mechanism will be called the resonance Stark effect. Both mechanisms may contribute. As is evident from

TABLE 1: Summary of Reduced Parameters and Their Corresponding Definitions

reduced param	corresponding definition
reduced energy variable	$\xi = (\nu - \nu_{CT})/\Delta_{CT}$
relative shift term	$\delta = (\nu_0 - \nu_{CT})/\Delta_{CT}$
relative coupling term	$R = V_0/\Delta_{CT}$
reduced dipole moment	$\Delta\vec{\mu}_R = \Delta\vec{\mu}_{CT}/\Delta_{CT}$
dimensionless vibrational overlap function	$g_2(\xi) = 2[(\ln 2)/\pi]^{1/2} \exp[-4(\ln 2)\xi^2]$
dimensionless dielectric function for CT state	$g(\xi) = g_1(\xi) + i\pi g_2(\xi)$

part 1 and Figure 1 in this paper, the expected higher order Stark effects due to $\Delta\mu_0$ for a monomeric BChl molecule is much smaller than the observed unusual higher order Stark effects for a BChl molecule in the RC. In the following, the resonance Stark effect is derived first by assuming $\Delta\mu_0$ to be zero; a derivation including the Liptay-type Stark effect due to a nonzero $\Delta\mu_0$ is given in the Appendix.

Resonance Stark Mechanism. The Stark effect is frequently only a perturbation to the dielectric function, so we use a perturbative approach to obtain the Stark effect on the dielectric function as

$$\Delta\epsilon(\nu) = \epsilon(\nu, F) - \epsilon(\nu) = \epsilon^2|V_0|^2\Delta G(\nu) + \epsilon^3[|V_0|^2\Delta G(\nu)]^2 + \epsilon^4[|V_0|^2\Delta G(\nu)]^3 + ... \quad (4)$$

where $\Delta G(\nu)$ is the change in $G(\nu)$ in an applied electric field F. $\epsilon(\nu)^k$ is directly proportional to the $(k-1)$th derivative of the dielectric function $\epsilon(\nu)$ with respect to ν (k is an integer). In the simplest picture, upon application of an electric field F, the energy of the CT state is shifted by $\Delta\nu_{CT} = -\Delta\vec{\mu}_{CT}\cdot\vec{F}$, where $\Delta\vec{\mu}_{CT}$ is the difference dipole vector between the ground and CT state. We will assume that neither the width Δ_{CT} of $G_2(\nu)$ nor its functional form (Gaussian) is affected by the applied electric field. If $\Delta\nu_{CT}$ is smaller than the line width Δ_{CT} of $G_2(\nu)$, $\Delta G(\nu)$ can be expanded as a Taylor series in $\Delta\nu_{CT}$:

$$\Delta G(\nu) = G(\nu, F) - G(\nu) = -G^{(1)}\Delta\nu_{CT} + \frac{G^{(2)}}{2!}\Delta\nu_{CT}{}^2 - \frac{G^{(3)}}{3!}\Delta\nu_{CT}{}^3 + ... \quad (5)$$

where $G^{(k)}$ is the kth derivative of $G(\nu)$ with respect to ν. For an immobilized and isotropic sample such as that typically used in Stark measurements,[4,6] any odd power field-dependent $\Delta\epsilon(\nu)$ vanishes, and $\Delta\epsilon(\nu)$ is generally written as

$$\Delta\epsilon(\nu) = \Delta\epsilon(\nu, F^2) + \Delta\epsilon(\nu, F^4) + \Delta\epsilon(\nu, F^6) + ... \quad (6)$$

where $\Delta\epsilon(\nu, F^n)$ ($n = 2, 4, 6, ...$) is the nth power field-dependent Stark effect of the dielectric function. Combining eqs 4−6 yields the theoretical resonance Stark effects of the dielectric function which have F^2, F^4, F^6, ... field dependencies.

For convenience, the following reduced variables are introduced, and they are summarized in Table 1. The reduced energy variable ξ is defined as $\xi = (\nu - \nu_{CT})/\Delta_{CT}$; the relative shift term δ is defined as $\delta = (\nu_0 - \nu_{CT})/\Delta_{CT}$; and the relative coupling strength R is $R = V_0/\Delta_{CT}$ (V_0 is understood as a real quantity here for simplicity). The reduced dipole moment $\Delta\vec{\mu}_R$ is defined as: $\Delta\vec{\mu}_R = \Delta\vec{\mu}_{CT}/\Delta_{CT}$. $G_2(\nu)$ is replaced by a normalized dimensionless function $g_2(\xi)$ which is defined as $g_2(\xi) = 2[(\ln 2)/\pi]^{1/2} \exp[-4(\ln 2)\xi^2]$. The dimensionless dielectric function $g(\xi)$ for the CT state is defined as $g(\xi) = g_1(\xi) + i\pi g_2(\xi)$, where $g_1(\xi)$ represents the Hilbert transform of $g_2(\xi)$. After some algebraic manipulation, the term that is quadratic in the field $\Delta\epsilon(\nu, F^2)$ is given as

$$\Delta\epsilon(\nu, F^2) = \left[\epsilon(\nu)^2(\Delta_{CT}R^2)\frac{g^{(2)}(\xi)}{2!} + \epsilon(\nu)^3(\Delta_{CT}R^2)^2(g^{(1)}(\xi))^2\right](\Delta\mu_R F)^2 C_{CT}^{2\omega} \quad (7a)$$

where an orientation average has been performed for an isotropic sample, $g^{(k)}$ (k is an integer) is the kth derivative of $g(\xi)$ with respect to ξ and $C_{CT}^{2\omega}$ is the resulting angle factor for this term, whose explicit expression will be given later. ω is the applied sinusoidal electric field frequency, so 2ω denotes the Stark effect for an isotropic sample that depends quadratically upon the applied field strength, while $n\omega$ denotes the higher order Stark effect that depends on the nth power of applied electric field strength.[4] The 4ω and 6ω higher order Stark effects are given as

$$\Delta\epsilon(\nu, F^4) = \left\{\epsilon^2(\Delta_{CT}R^2)\frac{g^{(4)}}{4!} + \epsilon^3(\Delta_{CT}R^2)^2\left[\left(\frac{g^{(2)}}{2!}\right)^2 + 2g^{(1)}\frac{g^{(3)}}{3!}\right] + \epsilon^4(\Delta_{CT}R^2)^3 3(g^{(1)})^2\frac{g^{(2)}}{2!} + \epsilon^5(\Delta_{CT}R^2)^4(g^{(1)})^4\right\}(\Delta\mu_R F)^4 C_{CT}^{4\omega} \quad (7b)$$

$$\Delta\epsilon(\nu, F^6) = \left\{\epsilon^2(\Delta_{CT}R^2)\frac{g^{(6)}}{6!} + \epsilon^3(\Delta_{CT}R^2)^2\left[\left(\frac{g^{(3)}}{3!}\right)^2 + 2\left(g^{(1)}\frac{g^{(5)}}{5!} + \frac{g^{(2)}}{2!}\frac{g^{(4)}}{4!}\right)\right] + \epsilon^4(\Delta_{CT}R^2)^3\left[\left(\frac{g^{(2)}}{2!}\right)^3 + 6g^{(1)}\frac{g^{(2)}}{2!}\frac{g^{(3)}}{3!} + 3(g^{(1)})^2\frac{g^{(4)}}{4!}\right] + \epsilon^5(\Delta_{CT}R^2)^4\left[6\left(g^{(1)}g\frac{g^{(2)}}{2!}\right)^2 + 4(g^{(1)})^3\frac{g^{(3)}}{3!}\right] + \epsilon^6(\Delta_{CT}R^2)^5(5)(g^{(1)})^4\frac{g^{(2)}}{2!} + \epsilon^7(\Delta_{CT}R^2)^6(g^{(1)})^6\right\}(\Delta\mu_R F)^6 C_{CT}^{6\omega} \quad (7c)$$

where ϵ is always a function of energy ν and $C_{CT}^{n\omega}$, $n = 4, 6, 8, ...$, is the angle factor described in the following.

As a result of mixing between the molecular exciton state and charge-transfer state, the final excited state gains its resonance-induced permanent dipole moment (and polarizabilities) from interaction with the charge-transfer state only (neglecting $\Delta\mu_0$ as discussed above). Therefore the resonance-induced dipole moment must share the same direction as that of the dipole moment ($\Delta\mu_{CT}$) of the CT state. On the other hand, the transition dipole moment to the final state, although not explicitly included in eq 7, is the same as that to the molecular exciton state from the ground state. Therefore, there exists an angle ζ_{CT} between this transition dipole and the resonance-induced permanent dipole moment.[8] For an isotropic sample, the Stark effect depends on the experimental angle χ between the probe light polarization and applied field directions, depending on the value of the internal angle ζ_{CT}.[5,6] The angle factor $C_{CT}^{n\omega}$ (n is a positive even integer) for the $n\omega$ Stark spectrum is readily derived when one performs the orientation average using Euler angles, yielding

$$C_{CT}^{n\omega} = \frac{1}{(n+1)(n+3)}\left[(n+3) + \frac{n}{2}(3\cos^2\chi - 1)(3\cos^2\zeta_{CT} - 1)\right], \quad n = 2, 4, 6, ... \quad (8)$$

It is important to notice in eq 7 that $C_{CT}^{n\omega}$ is a *multiplicative* constant for each ϵ^k term in any HOS spectrum, so only the *amplitude*, not the *line shape*, of the HOS spectrum should change when the experimental angle χ is changed. A special

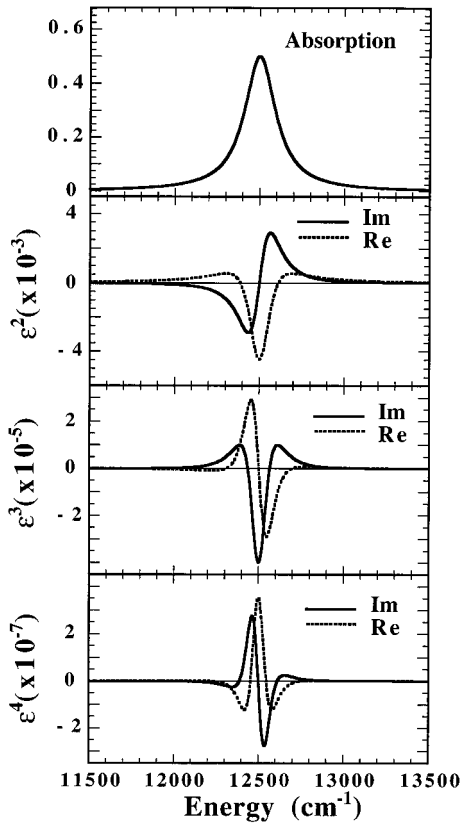

Figure 3. Imaginary (solid line) and real (dotted line) parts of various power dependencies of the dielectric function $\epsilon(\nu)$ are shown, calculated from eq 3 and scaled by the same constant so that the peak absorbance is 0.5. These derivative line shapes are weighted differently by physical parameters that contribute to the resonance Stark effect.

situation arises if ζ_{CT} is the magic angle, as $C_{CT}^{n\omega}$ becomes a constant that depends only on n, and then neither the amplitude or the line shape of higher order Stark spectra depends on χ. In conclusion, the angle dependence of the resonance HOS effect can be used to deduce the angle ζ_{CT} between the transition dipole direction and the permanent dipole direction of the CT state, which is essentially the charge-transfer direction.

Qualitative Analysis of Resonance Stark Line Shapes. To analyze experimental higher order Stark spectra, one needs to compute the imaginary parts of $\Delta\epsilon(\nu)$ in eq 7. The explicit analytical forms of the imaginary parts of $\Delta\epsilon(\nu)$ are very tedious, and it is much more convenient to obtain the imaginary part of eq 7 numerically. A significant advantage of using the complex dielectric function lies in its formal simplicity so that a physical understanding can be developed as follows. There are two factors in eq 7 that affect the HOS line shapes: the coupling strength $\Delta_{CT}R^2$, which is proportional to the broadening term $\pi(|V_0|^2/\Delta_{CT})g_2(\xi)$ at $\xi = \xi_0$, and the derivatives of the dimensionless function $g(\xi)$. The term $\Delta\mu_R F$ and the angle factor $C_{CT}^{n\omega}$ only affect the overall *amplitude*, not the *line shape*, of any HOS spectrum so these will be considered in a later section.

For simplicity, we use the imaginary part of eq 3, that is, a Lorentzian line shape in the weak charge resonance limit, to approximate an experimental absorption line shape. Although this simplification may preclude a perfect line shape agreement with experimental data, it will not affect the line shape relationship among the absorption and its HOS spectra, as will become evident below. The imaginary and real parts of $\epsilon(\nu)$ and their derivatives are calculated from eq 3 and are shown in Figure 3. To build in the connection with the unusual B band HOS effects reported in part 1, ν_0 is chosen as 12 500 cm^{-1}, Γ_0 as 110 cm^{-1}, and R as zero. For these parameters, the Γ term (hwhm, half width at half-maximum), given by the sum of Γ_0 and $\pi|V_0|^2G_2(\nu)$ (at $\nu = \nu_0$), is 110 cm^{-1}, which reasonably approximates the experimental B_L absorption line width.[9]

Figure 3 shows that the real and imaginary parts of any ϵ^k (k = 1, 2, ...) have similar amplitudes. A higher order power dependence of $\epsilon(\nu)$, i.e., a higher order derivative of $\epsilon(\nu)$, has a smaller amplitude and narrower line shape than a lower order power dependence of $\epsilon(\nu)$. Because the amplitude ratio between the imaginary (or real) parts of $\epsilon(\nu)^{k+1}$ and $\epsilon(\nu)^k$ is proportional to $1/\Gamma$, the relative contribution from the imaginary (or real) parts of the $\epsilon(\nu)^{k+1}$ term and the $\epsilon(\nu)^k$ term to $\Delta\epsilon(\nu,F^n)$ in eq 7 is proportional to $\Delta_{CT}R^2/\Gamma$. If the condition $\Delta_{CT}R^2 \ll \Gamma$ applies, eq 7 can be drastically simplified to

$$\Delta\epsilon(\nu,F^n) \approx \epsilon(\nu)^2(\Delta_{CT}R^2)\frac{g^{(n)}(\xi)}{n!}(\Delta\mu_R F)^n C_{CT}^{n\omega}, \quad n = 2, 4, 6, \ldots \quad (9)$$

It is evident from eq 9 that the contribution from the $\epsilon(\nu)^2$ term with the *lowest order* derivative line shape will dominate all the resonance HOS spectra, and they should *all* have similar line widths. On the other hand, if the $\Delta_{CT}R^2$ term becomes larger relative to Γ, there will be a relatively greater contribution from higher order derivative (narrower) line shapes and eq 9 no longer applies. For a given experimental absorption line width Γ, the coupling term $\Delta_{CT}R^2$ alone determines whether a lower order derivative line shape (broader) or higher order derivative line shape (narrower) will dominate the higher order Stark spectra. The actual absorption line shape (whether a Lorentzian or Gaussian) will not affect this conclusion.

The physical meanings of $g^{(k)}(\xi)$ in eqs 7 and 9 can be understood as follows. In the weak charge resonance limit, appreciable absorption to the final state takes place only in the vicinity of the exciton-state energy ν_0. Because the absorption line width Γ is expected to be much smaller than the vibrational overlap bandwidth Δ_{CT} of $G_2(\nu)$ (*cf.* Figure 2), one only needs to consider the *local* values of the derivatives of $G(\nu)$ in the vicinity of $\nu = \nu_0$ in order to understand the main features of the absorption and HOS spectra in this limit. In the reduced coordinates this means that only the local values of the derivatives of $g(\xi)$ in the vicinity of $\xi = \delta$ need to be considered, which can be viewed as constants. As seen from eq 2, $|V_0|^2G_1(\nu)$, or equivalently $\Delta_{CT}R^2g_1(\xi)$, is the resonance energy shift term which determines the absorption peak location. Upon application of the electric field F, the absorption peak shift is given as

$$(\Delta_{CT}R^2)\Delta g_1(\xi) = -(\Delta_{CT}R^2)g_1^{(1)}\Delta\vec{\mu}_R\cdot\vec{F} + (\Delta_{CT}R^2)\frac{g_1^{(2)}}{2!}(\Delta\vec{\mu}_R)^2:(\vec{F})^2 - \ldots \quad (10)$$

The first term on the right side depends linearly on applied field strength, so $(\Delta_{CT}R^2)g_1^{(1)}\Delta\vec{\mu}_R$ can be defined as the resonance-induced dipole moment, which lies parallel to the direction of $\Delta\vec{\mu}_{CT}$, as expected. The second term has a quadratic field dependence, so $(\Delta_{CT}R^2)(g_1^2/2!)(\Delta\vec{\mu}_R)^2$, a second rank tensor, corresponds to the resonance-induced polarizability tensor (":" denotes a tensor calculation in eq 10). Other higher order terms in eq 10 can be similarly defined as higher order resonance-induced polarizability tensors. Analogous to eq 10, Taylor expansion can be applied to the resonance-induced broadening

TABLE 2: Explicit Expressions for Complex Resonance-Induced Dipole Moments and Polarizabilities

resonance-induced dipole and polarizabilities	expressions for eq 7	expressions for eq 12
$\Delta\vec{\mu}$	$\Delta_{CT}R^2 g^{(1)}\Delta\vec{\mu}_R$	$\Delta_{CT}R^2 g^{(1)}\Delta\vec{\mu}_R + \Delta\vec{\mu}_0$
$\hat{\alpha}^{(k)}$, $k \geq 2$	$\Delta_{CT}R^2\frac{g^{(k)}}{k!}(\Delta\vec{\mu}_R)^k$	same as left

term $\pi\Delta_{CT}R^2 g_2(\xi)$ to obtain its responses to an applied electric field (not shown).

For convenience, we can define the complex dipole moment and polarizability tensors in terms of $g^{(k)}$ as shown in Table 2: their real parts are related to how the applied field affects the energy of the final state, while their imaginary parts are related to how the applied field affects the lifetime of the final state. As the relative location ($\xi = \delta$) of the exciton state within the CT vibronic continuum is changed, $g^{(k)}(\xi)|_{\xi=\delta}$ changes accordingly. Consequently the resonance-induced dipole and polarizabilities will change and result in changes to the resonance higher order Stark spectra according to eq 7 (or eq 9). This has important physical implications. In real systems the exciton-state energy (ν_0) often varies little; for example the B band locations in different RCs (see part 1), whereas the energy of a CT state should be very sensitive to local environmental perturbations. Therefore, the value of δ is most directly influenced by the energy of the coupled CT state. A more negative δ value corresponds to a higher energy for the CT state and a smaller driving force for charge transfer from the molecular exciton state to the CT state in the usual Marcus theory formulation.[10] As the value of δ changes, we expect the resonance-induced polarizabilities for the *D state (near $\nu = \nu_0$) to vary according to the definitions in Table 2. Therefore resonance HOS spectra are informative about the energetics for excited-state charge transfer.

To see qualitatively how δ affects the resonance HOS line shape, we examine the limiting case where the condition $\Delta_{CT}R^2 \ll \Gamma$ is met and eq 9 is applicable. This limiting case should be frequently applicable in the weak charge resonance limit where electron-transfer dynamics are often studied by time-resolved spectroscopy. The imaginary part of eq 9 has the following form

$$\Delta\epsilon_2(\nu, F^n) \propto Im(\epsilon^2)\, Re(\alpha^{(n)}) + Re(\epsilon^2)\, Im(\alpha^{(n)}), \quad n = 2, 4, 6, \ldots \quad (11)$$

where the resonance-induced complex polarizability $\alpha^{(n)}$ is defined in Table 2. The imaginary and real parts of $\epsilon(\nu)^2$ always have similar amplitudes, but very different line shapes (see Figure 3). Specifically, $Im(\epsilon^2)$ has a band-shift line shape which is weighted by $Re(\alpha^{(n)})$, that is, a measure of the nth order field-induced change in energy (see eq 10 and Table 2). On the other hand, $Re(\epsilon^2)$ has a band-broadening line shape which is weighted by $Im(\alpha^{(n)})$, that is, a measure of the nth order field-induced lifetime broadening (or narrowing depending on its sign). Evidently, a competition exists between these two completely different line shape contributions to any $n\omega$ Stark spectrum. Figure 4 shows the energy dependence (in reduced coordinates) of various resonance-induced polarizabilities. It is expected, and verified later through numerical analysis, that there will be a smooth variation in the line shape of any $n\omega$ Stark spectrum as δ varies. In experimental systems this variation of δ is due to changes in the D^+A^- state energy by changing the D/D^+ and/or A/A^- redox potentials or by changing the environment so as to differentially stabilize or destabilize the D^+A^- state.

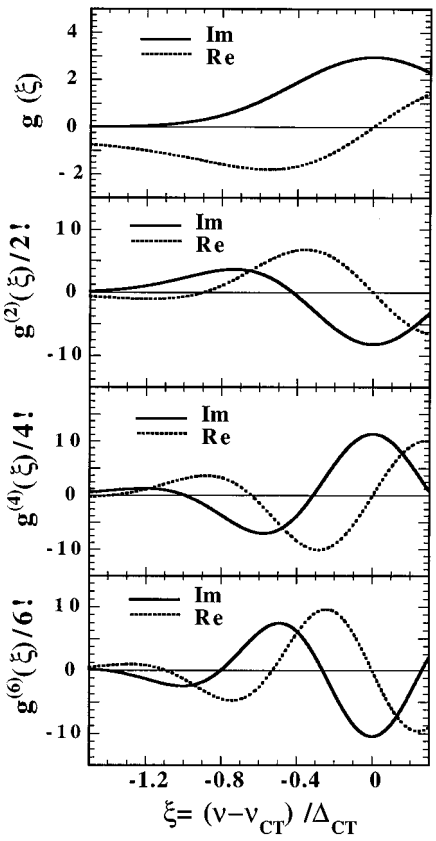

Figure 4. Imaginary (solid line) and real (dotted line) parts of the nth derivatives of the dimensionless function $g(\xi)$. These represent the energy dependence of the resonance-induced nth order polarizabilities according to Table 3. ξ is the reduced energy variable (Table 1).

As discussed above, the actual $n\omega$ Stark line shape depends only on the relative contribution from the real and imaginary parts of $g^{(n)}$ at $\xi = \delta$ (see eq 11 and Table 2). One notices that the value of $Im(g^{(n+2)})$ *often* has the opposite sign to that of $Im(g^{(n)})$ at $\xi = \delta$ (see Figure 4). Such sign alternation is *often* true between $Re(g^{(n)})$ and $Re(g^{(n+2)})$ as well. Furthermore, the relative values of $Re(g^{(n)})$ and $Im(g^{(n)})$ are similar for different n values. Therefore, we expect that the $(n + 2)\omega$ Stark spectrum should *approximately* resemble an inverted $n\omega$ Stark spectrum in many cases.

In summary, the relative values of the coupling strength $\Delta_{CT}R^2$ and the absorption line width Γ determine whether the resonance higher order Stark spectra are lower-order derivative-like (relatively broader) or higher order derivative-like (relatively narrower), from which we obtain information on the coupling strength. The relative shift term δ determines the actual line shape of any HOS spectrum, i.e., whether the HOS spectrum line shape resembles a band-shift or band-broadening. As δ is varied, the HOS spectra are expected to show a continuous line shape variation, and this variation provides information on the relative energy between the molecular exciton and the CT state. The effect of the $\Delta_{CT}R^2$ term on HOS line shapes is *independent* of the effect of δ. For $\Delta_{CT}R^2 \ll \Gamma$, all HOS spectra would show lower order derivative line shapes according to eq 9, and we expect an approximate line shape "inversion" between $n\omega$ and $(n + 2)\omega$ Stark spectra. Examples of these variations will be presented below in the comparison of experimental and calculated line shapes and amplitudes.

Data analysis Methodology for Resonance Stark Spectra. When $\Delta_{CT}R^2 \ll \Gamma$, the value of δ determines the line shape for all $n\omega$ resonance Stark effects *simultaneously*. As an internal test of the theory, δ is adjusted until a simultaneous line shape

agreement is obtained for every $n\omega$ Stark effect for a particular system. Higher order Stark effects are essential, not just because they allow identification of the resonance Stark mechanism but also because the contribution from conventional Stark effects (Liptay-type, see Appendix) may mask the resonance Stark effect for a lower order spectrum. Furthermore, other useful physical parameters, such as coupling strength $\Delta_{CT}R^2$, can be extracted from the *amplitudes* of higher order Stark effects as discussed in the following.

When $\Delta_{CT}R^2 \ll \Gamma$ there should be a regular line shape variation (approximate sign inversion) between the $n\omega$ and $(n + 2)\omega$ Stark spectra. Therefore the relative amplitudes of the $n\omega$ and $(n + 2)\omega$ Stark spectra are meaningful and directly yield information on the $(\Delta\mu_R F)^2$ term (see eq 9). The value of $\Delta_{CT}R^2$ can then be obtained as follows: The amplitude of the $n\omega$ Stark spectrum for a given absorption amplitude is directly proportional to the product of $\Delta_{CT}R^2$ and $(\Delta\mu_R F)^n$ (see eq 9). Once $(\Delta\mu_R F)^2$ is known from an amplitude comparison between any two $n\omega$ and $(n + 2)\omega$ HOS spectra, then $\Delta_{CT}R^2$ can be obtained directly by comparing any $n\omega$ Stark spectrum with the absorption spectrum. Therefore, from the amplitudes of resonance Stark effects, we have another internal consistency test for the weak coupling condition $\Delta_{CT}R^2 \ll \Gamma$. This simple method is no longer valid if a higher order Stark spectrum has a higher order derivative line shape; however, it is clear from eq 7 that a quantitative analysis is still possible because the parameters maintain their distinct physical meanings and lead to different consequences.

Results

General Features of HOS Line Shapes and Amplitudes. In part 1, it was found that all HOS spectra in the B band region have lower derivative (broad) line shapes with similar line widths and that there is an approximate line shape inversion relationship between each pair of 4ω and 6ω Stark spectra. As shown by the comparison in Figure 1 for the spectrally simple case of *C. aurantiacus* RCs, these HOS features cannot be explained by the conventional Liptay-type Stark mechanism. As discussed qualitatively above, they are readily understood as resonance Stark effects if the weak coupling limit $\Delta_{CT}R^2 \ll \Gamma$ is satisfied where the molecular exciton state is understood to be the ^1B_L state, and, on the basis of variations seen in part 1, the coupled CT state involves charge transfer between B_L and H_L.

The theoretical absorption spectrum is taken as the imaginary part of eq 3 scaled by a multiplicative constant such that the peak absorbance is 0.5, and ν_0 is chosen as 12 500 cm^{-1}. The same multiplicative constant is used for $\epsilon(\nu)$ in calculating resonance Stark effects based on eq 9. The Γ_0 term is chosen as 110 cm^{-1} which best approximates the experimental B_L absorption line width (see Figure 1) for the condition $\Delta_{CT}R^2 \ll \Gamma_0$. The angle ζ_{CT} between the transition dipole moment and the CT direction is approximately the magic angle because the novel HOS line shapes and amplitudes in the B band region show little dependence on the experimental angle χ (see Figures 3C and 4 in part 1). These parameters are specific to the B band Stark effect in the RCs, and they would be different but similarly obtainable from experimental data for other DA systems. The remaining parameters of interest are Δ_{CT} and δ. Δ_{CT} is related to the reorganization energy in conventional electron-transfer theories,[10−13] and it is expected to be much greater than the B_L absorption bandwidth. As an initial choice we set Δ_{CT} to be 1600 cm^{-1}, and this choice will be addressed following examination of the dependence of resonance Stark effect line shapes on the value of δ based on eqs 3 and 9.[14] The effective coupling strength $\Delta_{CT}R^2$ is taken as 6 cm^{-1}, and the $\Delta\mu_R F$ term is chosen as 0.68. Effects of varying these parameters will also be discussed below.

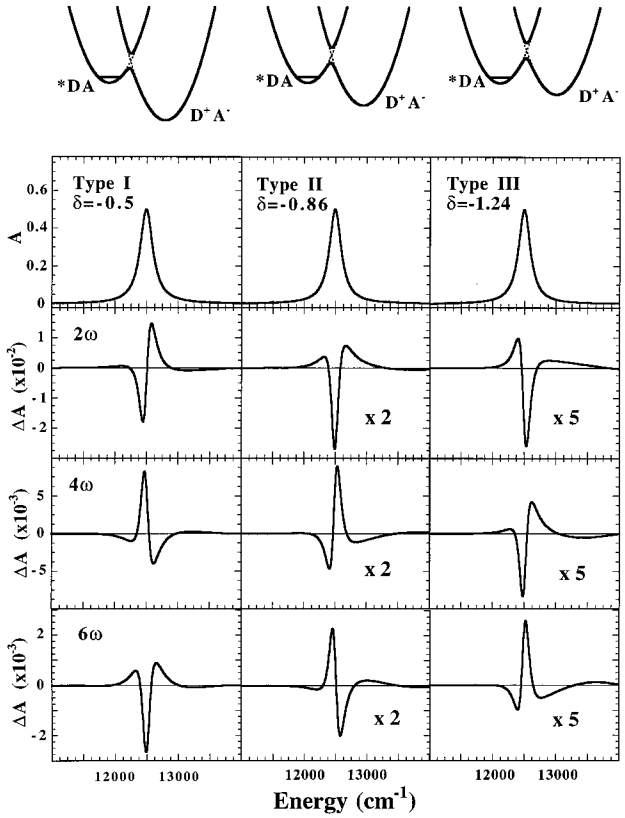

Figure 5. Calculated resonance Stark effects for the three classification types discussed in the text varying only the parameter δ as indicated. The values of other parameters are as follows: $\Delta_{CT}R^2 = 6$ cm^{-1}; $\Delta\mu_R F = 0.68$; $\nu_0 = 125\,00$ cm^{-1} (appropriate for B in the reaction center). The more familiar potential energy diagram corresponding to the variation in δ is shown at the top, where the charge-transfer state potential surface is lowest in energy for type I, higher for type II, and highest for type III, leading to the largest driving force for electron transfer in type I and smallest for type III. Only the value of δ was varied by changing ν_{CT}.

Figure 5 shows a series of theoretical resonance Stark spectra with only the parameter δ being varied. It is seen that several of these line shapes closely resemble the observed higher order Stark effects of the B band in various RCs in part 1. There the various types of spectra were classified as types I−III, and these can be approximately simulated when δ is chosen to be −0.5, −0.86, and −1.24, respectively, as discussed in detail below. Each set of simulated $n\omega$ resonance Stark effects shares the same vertical axis on the left, but their actual amplitudes are not the same. For any $n\omega$ Stark effect, the amplitude is always largest for type I, smaller for type II, and smallest for type III. This means that the *D state in type I is most polarizable, while it is less polarizable in type II and least polarizable in type III. All resonance Stark spectra have similar line widths, and each exhibits either a band-broadening (or narrowing) line shape due to a field-induced lifetime change or a band-shift line shape due to field-induced energy change. For the type I Stark effect, the 2ω Stark spectrum has mostly a *blue*-shifted line shape, with some contribution from a band-broadening line shape. The 4ω Stark spectrum shows mostly a band-narrowing line shape, somewhat resembling an inverted 2ω Stark line shape, but more centrosymmetric. This trend is continued from the 4ω to the 6ω Stark line shape: the 6ω Stark spectrum is approximately

an inverted 4ω spectrum, with the 6ω Stark spectrum more centrosymmetric than the 4ω Stark spectrum. For the type II Stark effect, the 2ω Stark spectrum has mostly a band-broadening line shape. The 4ω Stark line shape resembles an inverted 2ω Stark line shape but has relatively more contribution from a band-shift line shape and becomes more asymmetric. Again, this trend is continued in the 6ω Stark line shape, which is even more asymmetric, but still resembles an inverted 4ω Stark line shape. For the type III Stark effect, the 2ω Stark spectrum has a *red*-shifted line shape, in contrast to the type I 2ω Stark effect. The 4ω Stark spectrum has a lower derivative line shape and the 6ω Stark line shape resembles, but is more centrosymmetric than, an inverted 4ω Stark line shape. None of these line shapes resembles a conventional Liptay-type Stark effect due to $\Delta\mu_0$ (see right panels in Figure 1).

Among any $n\omega$ Stark spectra for these three types, there exists a gradual line shape variation from one to another as δ varies. Comparison with any experimental $n\omega$ Stark spectrum essentially allows a unique determination of the value of δ if other parameters are constant. We will argue below that it is physically reasonable that only δ changes appreciably for the RC variants for which data have been obtained. Further, a single δ value should *simultaneously* determine every $n\omega$ Stark spectrum of a given sample, and this provides a stringent test of the theory and makes line shape analysis straightforward. Once δ is chosen, $\Delta_{CT}R^2$ and $\Delta\mu_R F$ (which only affect amplitudes when eq 9 is used) can be uniquely determined from experimental Stark effect and absorption amplitudes as discussed above. Since a more negative δ value corresponds to a higher energy for the CT state, the CT state energy increases from type I to type III relative to the energy of the initial excited state. This corresponds to a continuous *decrease* in charge-transfer driving force in the familiar Marcus theory,[10] as illustrated qualitatively by the potential surface diagrams at the top of Figure 5. In the normal region of Marcus theory, as the driving force decreases, the charge-transfer rate decreases. This corresponds to the transition from type I to III with a concomitant decrease in polarizability of the *D state evident from the amplitudes of resonance Stark effects. Finally, the value of δ and the coupling strength $\Delta_{CT}R^2$ completely determine the lifetime broadening term, $\pi\Delta_{CT}R^2 g_2(\xi)|_{\xi=\delta}$ which can be used to estimate the electron-transfer rate from the uncertainty principle.

Effect of Δ_{CT} on Resonance Stark Line Shapes. Δ_{CT} is related to the reorganization energy in the usual terms of Marcus theory. To estimate the change in the driving force from the initial exciton state to the CT state from one type of resonance Stark spectrum to another, it is necessary to convert the value of δ into a real energy unit, and this requires knowledge of Δ_{CT}. A simulation illustrating the effect of varying Δ_{CT} is shown in Figure 6, where the 6ω Stark spectrum of type II ($\delta = -0.86$) is used as an example (the 6ω Stark effects are mainly due to the resonance Stark effect). It is seen that variation in Δ_{CT} has little effect on the sharp and dominant Stark line shape; however, a larger value of Δ_{CT} leads to a more flattened Stark feature at higher energy around 13 000 cm^{-1}. Qualitatively, this can be understood as follows: quantum interference between a discrete (allowed) transition to the molecular exciton state near $\nu = \nu_0$ and a vibronically broad CT state (dark) makes the transition from the ground state to the CT state partially allowed.[1] Therefore we expect a broad Stark effect (due mostly to the CT state) to appear on the higher energy side of the narrow Stark features (due mostly to the exciton state). As shown in Figure 6, the line shape of this broad Stark feature is sensitive

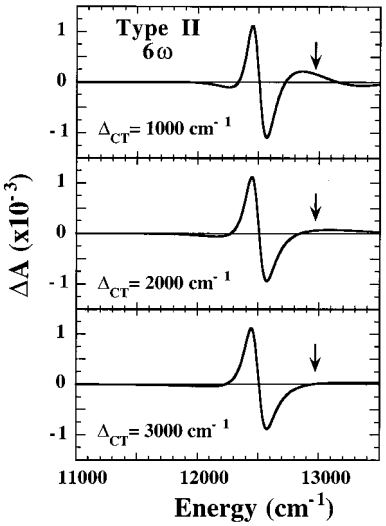

Figure 6. Effect of varying Δ_{CT} on a type II ($\delta = 0.86$) 6ω Stark spectrum. The values for $\Delta_{CT}R^2$ and $\Delta\mu_R F$ are kept the same as in Figure 5 by adjusting the values of V_0 and $\Delta\mu_{CT}$. The broad Stark feature around 13 000 cm^{-1} (see arrow) broadens as Δ_{CT} becomes larger.

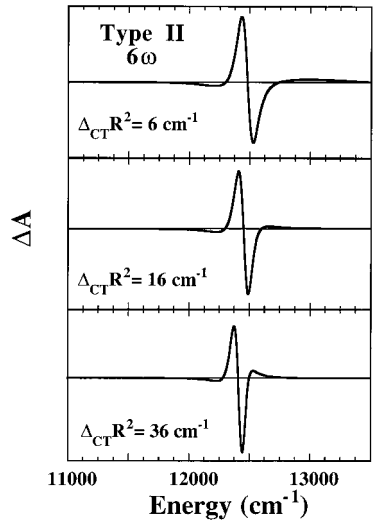

Figure 7. Effect of a varying the relative coupling strength $\Delta_{CT}R^2$ on a type II 6ω Stark spectrum. The line shape becomes sharper as $\Delta_{CT}R^2$ increases. Δ_{CT} is held constant, so this is the effect of varying the electronic coupling V_0 (see Table 1).

to the value of Δ_{CT}. Therefore, we can estimate the Δ_{CT} value by simulating this broad Stark feature of an experimental Stark spectrum and obtain the relative driving force for electron transfer.

Effect of Larger Relative Coupling. In the above, we have focused on the weak coupling condition $\Delta_{CT}R^2 \ll \Gamma_0$, chosen such that all $n\omega$ Stark spectra have similar line widths. As discussed qualitatively in the theory section, a larger coupling relative to $\Delta_{CT}R^2$ for the same Γ_0 should yield a higher order derivative line shape for a higher order Stark spectrum. This is illustrated quantitatively in Figure 7, again using the 6ω Stark spectrum of type II ($\delta = -0.86$) as an example, calculated from the exact solution of eq 7. Three values of $\Delta_{CT}R^2$ are chosen with the absorption width $\Gamma = \Delta_{CT}R^2 + \Gamma_0$ fixed to be 110 cm^{-1}. Since we are only interested in line shape changes, not the amplitude, $\Delta\mu_R F$ can be chosen arbitrarily such that the calculated 6ω Stark spectra share a similar amplitude to facilitate line shape comparison (for this reason the vertical scales in Figure 7 are left off). As expected, a sharper, higher order derivative line shape is found for a larger coupling $\Delta_{CT}R^2$ term.

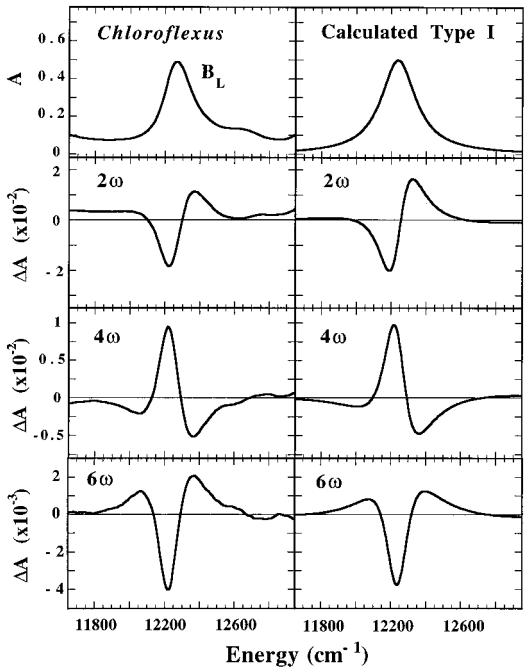

Figure 8. Comparison between experimental HOS spectra for *Chloroflexus aurantiacus* RCs and simulations using eq 9 for $\delta = -0.50$ and the parameters in Table 3. The same set of parameters is used for the 2-, 4-, and 6ω spectra. Similar parameters apply to the (M)Y210F mutant of *Rb. sphaeroides*.

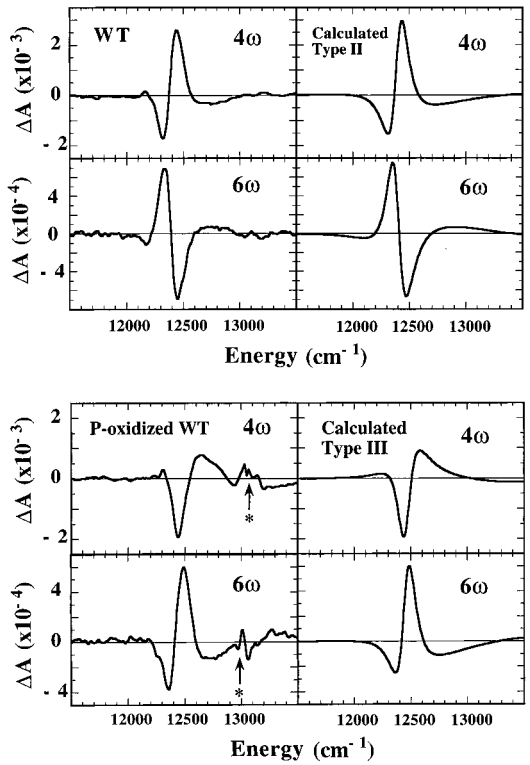

Figure 9. Comparison between experimental 4ω and 6ω spectra for wild-type *Rb. sphaeroides* (upper set) and P-oxidized wild-type *Rb. sphaeroides* (lower set) and simulations using eq 9 and the parameters shown in Table 3. In contrast to *Chloroflexus aurantiacus* RCs in Figure 8, the 2ω experimental Stark spectra have significant contributions from Liptay-type Stark mechanism (see Appendix), but no attempt was made to fit these.

Because the experimental B band higher order Stark effects observed to date all have similar broad line widths and lower order derivative line shapes, it appears that $\Delta_{CT}R^2 \ll \Gamma_0$ and the approximate solution in eq 9 is sufficient to simulate the experimental data. In this limit, only the value of δ affects the HOS line shapes as discussed above. The coupling strength $\Delta_{CT}R^2$ is extracted from an analysis of resonance Stark effect and absorption amplitudes.

Comparison between Theory and Experiment. Figure 8 shows a simulation of the Stark effects of B_L in WT *C. aurantiacus* RCs, which falls into type I. The agreement for the shape and amplitude for each $n\omega$ Stark spectrum is excellent, indicating that the basic model is valid and that reliable parameters can be obtained (see Table 3). Qualitatively similar B band HOS spectra were observed for the (M)Y210F mutant of *Rhodobacter* (*Rb. sphaeroides*) RCs (see part 1, Figure 10), and the results of simulations (not shown) are given in Table 3.

For both types II and III the 2ω Stark spectra are substantially weaker than for type I, and they contain a significant contribution from the Liptay-type mechanism (see Appendix). In this case we make comparisons with the extracted, unusual higher order Stark effects for the B band (see part 1) and only the 4ω and 6ω spectra. Figure 9A shows a comparison between the resonance 4ω and 6ω Stark spectra for WT *Rb. sphaeroides* RCs (part 1, Figure 5) and the calculated 4ω and 6ω type II HOS spectra. Similar B band Stark effects were observed for P-oxidized (M)Y210F RCs of *Rb. sphaeroides* (see Figure 10, part 1), which is also classified as a type II Stark effect (parameters for both are given in Table 3). The relative coupling strength $\Delta_{CT}R^2$ obtained for P-oxidized (M)Y210F RC is somewhat larger than that for WT *Rb. sphaeroides* RC, because the magnitude of the resonance Stark effect in P-oxidized (M)-Y210F RCs is found to be larger. Figure 9B shows a simulation of the type III Stark spectra for *Rb. sphaeroides* RCs with the special pair chemically oxidized to P^+ (Figure 8, part 1). As discussed above, Δ_{CT} affects the breadth of the feature on the higher energy side of the main Stark effect. The resonance Stark effect always dominates the 6ω B band Stark effect, so in this case Δ_{CT} was adjusted so that a close line shape agreement is found between data and simulation. This gives a value of Δ_{CT} estimated to be 1600 cm^{-1}. The impact of Δ_{CT} in this range is modest (Figure 6), so this is the least well-defined parameter at this time. Using this value and the estimated values of δ, the difference in CT state energy from type I to II, or from type II to III, is about 640 cm^{-1}. The absolute energy of the coupled CT state is not obtained from this treatment; however, *changes* in energy associated with chromophore or environmental perturbations are very useful and can be compared with theoretical estimates. The treatment does allow the *lifetime* of excited-state electron transfer to be estimated from the resonance

TABLE 3: Parameters Used in Calculating Resonance Stark Spectra in Figures 8 and 9 from Equations 3 and 9

reacn centers	δ	$\Delta_{CT}R^2$ (cm^{-1})	$\Delta\mu_R F$	$\pi\|V_0\|^2G_2(\nu_0)$ (cm^{-1})	ν_0 (cm^{-1})	electron-transfer lifetime (ps)
C. aurantiacus	−0.50	6.0	0.72	9	12 250	0.6
(M)Y210F of *Rb. sphaeroides*	−0.50	6.1	0.72	9	12 400	0.6
wild-type *Rb. sphaeroides*	−0.86	4.1	0.68	1.6	12 400	3.3
P-oxidized (M)Y210F of *Rb. sphaeroides*	−0.84	6.0	0.68	2.2	12 400	2.4
P-oxidized wild-type *Rb. sphaeroides*	−1.26	6.6	0.7	0.24	12 457	22

broadening term $\pi(\Delta_{CT}R^2)g_2(\xi)$ at $\xi = \delta$ using Fermi's Golden rule and the uncertainty principle, and the estimated values are given in Table 3. Finally, we can use the estimated value of Δ_{CT} to obtain an estimate for the electronic coupling V_0 from the relative coupling $\Delta_{CT}R^2$ using $R = V_0/\Delta_{CT}$ (Table 1). Taking a typical value for $\Delta_{CT}R^2 = 6$ cm^{-1} (Table 3), V_0 is approximately 100 cm^{-1} for $^1B_L \rightarrow B_L^+H_L^-$.

Discussion

Physical Picture of the Resonance Stark Effect. In the traditional Liptay theory, the absorption line shape is assumed to be unchanged by the applied electric field.[5,6] The Liptay-type Stark effect arises from the interaction of the difference dipole moment (or polarizability) with the applied electric field which results in a change in transition energy. This picture is sufficient for most molecular systems where intermolecular interactions leading to electron transfer are negligible. The resonance Stark effect discovered in the photosynthetic RC is, on the other hand, intimately related to intermolecular charge-transfer dynamics. Both the energy and lifetime of the initial excited state due to charge transfer are affected by the applied electric field, and the resonance Stark effect is dynamic in nature.

The physical distinction between these two mechanisms is significant and can be further understood from the following one-electron picture. The first excited state of an isolated chromophore such as BChl can be viewed as a molecular exciton state, an electron−hole pair, which is strongly bound because of its large ionization potential. For the largest laboratory electric fields that can be applied (typically around 1 MV/cm or 100 mV/10 Å), the electrostatic energy from the external field is too weak to compete against the much stronger binding energy of the molecular exciton state. In this case, the static picture in Liptay theory is sufficient to account for the higher order Stark effects of an isolated molecule such as BChl, and this is found experimentally.[4] This situation is drastically changed when an intermolecular charge resonance interaction becomes significant as this effectively reduces the binding energy of the molecular exciton state of the electron donor which becomes much more polarizable.

We have developed a theory of the resonance Stark effect in terms of excited-state electron transfer and have shown that line shapes corresponding to experimental observations are predicted. For a given electronic coupling between a donor and acceptor pair with fixed intermolecular separation and reorganization energy, the energy of the molecular exciton state within the CT vibronic continuum changes if the redox potential of D and/or A changes or if the energy of D^+A^- changes due to environmental perturbations such as local amino acid residue changes or hydrogen-bonding. Concomitantly, the polarizability of the initial molecular exciton state changes. This results in a variety of different resonance Stark line shapes, which in turn provide information on the excited-state charge-transfer process. Interestingly, a rather regular pattern in the resonance-induced polarizabilities leads to characteristic regularities in the resonance Stark effects such as an approximate line shape "inversion" relationship among the $n\omega$ and $(n + 2)\omega$ Stark spectra when $\Delta_{CT}R^2 \ll \Gamma$. This weak coupling limit should be frequently applicable to photoinduced electron-transfer systems.

The functional form of $G_2(\nu)$ deserves further discussion. According to linear electron−phonon coupling theory, it should have an approximately Gaussian line shape.[13,15] In particular, its lower energy side can be approximated by a Gaussian, and this corresponds to the normal region in Marcus electron-transfer theory.[10] The higher energy side (the Marcus inverted region) may deviate substantially from this Gaussian line shape. At least for the cases found thus far for the B_L band in the RC, this does not affect any of our conclusions because the negative δ values found from analysis of the B band resonance Stark effects (see Table 3 and Figure 2) correspond to the normal region of Marcus theory, and the resonance Stark effect is only sensitive to the local value of $G_2(\nu)$ near the initial molecular exciton-state energy.

Evidence Supporting $^1B_L \rightarrow B_L^+H_L^-$. The comparison of Stark data for various RCs in part 1 suggests that intermolecular charge-transfer states involving B_L and H_L coupled to ^1B_L excitation are responsible for the unusual HOS effects, and the excellent agreement between data and theory developed for such a generic process ($^*D \rightarrow D^+A^-$ or D^-A^+) supports this. In addition, as shown in part 1, the resonance Stark effect for the B band has little dependence on the experimental angle χ. This means that the angle Δ_{CT} between the transition dipole moment for the B_L Q_y transition and the electron-transfer direction between B_L and H_L must be close to the magic angle (see eq 8). This angle can be estimated from the X-ray structure.[16] The permanent dipole moment for the $B_L^+H_L^-$ (or $B_L^-H_L^+$) state can be estimated from the center-to-center direction of the BChl and BPhe macrocycles; the transition dipole moment of the B_L band is believed to lie approximately along the line connecting the nitrogen atoms of rings I and III (N1−N3). The angle between these two lines is very close to the magic angle.

It is important to identify whether the $B_L^+H_L^-$ state or the $B_L^-H_L^+$ state is involved. Because BPhe is much easier to reduce and harder to oxidize in vitro than BChl,[17] the $B_L^+H_L^-$ state in RCs is likely lower in energy than the $B_L^-H_L^+$ state; however, either the $B_L^+H_L^-$ or the $B_L^-H_L^+$ state may be energetically closer to and interacts more strongly with ^1B_L a priori. A choice can be made on the basis of a correlation among the three types of observed resonance Stark effects and the nature of the perturbation for different RC variants. As defined in Table 1 (also see Figure 2), ν_{CT} is the peak location of $G_2(\nu)$ [not the actual energy of the CT state which is usually taken as the potential energy minimum and is still lower]. If ν_{CT} is larger than the actual CT state energy by a fixed amount (assuming Δ_{CT} is unchanged), then the change in δ value is directly proportional to the change in the CT state energy with a proportionality constant $-1/\Delta_{CT}$. A more negative value of δ corresponds to a higher CT state energy and is associated with the evolution from the type I to type III Stark effects. Experimentally, oxidation of P shifts the resonance Stark line shape from type II to III in wild-type *Rb. sphaeroides* and from type I to type II in the (M)Y210F mutant of *Rb. sphaeroides*. A positive charge on P should increase the energy of the $B_L^+H_L^-$ state, while decreasing the energy of the $B_L^-H_L^+$ state because P is physically much closer to B_L than to H_L. Therefore, we conclude, on the basis of the effects of oxidation of P, that the observed resonance Stark effect is due to a dominant interaction between ^1B_L and $B_L^+H_L^-$. Other variants are discussed in the following and confirm this conclusion. Significantly, the oxidation of P to P^+ produces approximately the same shift in δ in WT and the (M)Y210F mutant. Thus, it appears that the perturbations are additive, and this approach offers a unique approach for obtaining quantitative information on enivironmental perturbations.

Effects of the (M)210 Mutation. As shown in part 1, the (M)Y210F mutant of *Rb. sphaeroides* shows a type I Stark effect, while a type II Stark effect is found for WT *Rb. sphaeroides*. If the $B_L^+H_L^-$ state is primarily involved as

concluded above, then this result requires that the $B_L^+H_L^-$ state is lower in energy in the (M)Y210F mutant than in wild-type; i.e., the driving force for $^1B_L \rightarrow B_L^+H_L^-$ electron transfer is larger in (M)Y210F than wild-type. The tyrosine residue at position (M)210 in WT *Rb. sphaeroides* has been widely studied both experimentally and theoretically.[18−21] Calculations suggest that the dipole on the phenol of tyrosine stabilizes B_L^- in the $P^+B_L^-$ state, while P^+ and H_L^- are more weakly affected.[21] Conversely, because these residue dipole moments are not free to reorient, this dipole should destabilize B_L^+ in the $B_L^+H_L^-$ state, and this destabilizing effect on B_L^+ should be removed when a phenylalanine is present in (M)Y210F.[22] One expects a similar result for *C. aurantiacus* RCs as the residue at this position is a leucine. Thus the energy of the $B_L^+H_L^-$ state should be lower in (M)Y210F (and *C. aurantiacus*) than in wild-type *Rb. sphaeroides* RCs. On the basis of the quantitative analysis above, the energy change to the $B_L^+H_L^-$ state caused by a tyrosine to phenylalanine mutation is estimated to be 640 cm^{-1} (or 80 meV). This change in driving force leads to an increase in the rate of $^1B_L \rightarrow B_L^+H_L^-$ by a factor of 5−6 (see Table 3). These results also suggest a shortcoming in the analysis of the effects of mutations at position M208 in *Rb. capsulatus* (equivalent to M210 in *Rb. sphaeroides*).[23] These investigators measured the effect on the ^1P decay kinetics only in terms of effects of changes at M208 on the P/P^+ oxidation potential. The results presented here demonstrate a substantially larger perturbation on the B_L/B_L^+ potential, and a parallel perturbation, though opposite in sign, can be expected on the B_L/B_L^- reduction potential, as predicted by free energy perturbation calculations.[21]

Effects of the (M)H214L Mutation (*β* Mutant). A type III 6*ω* Stark effect was found in the B band region in the *β*-mutant (part 1, Figure 9). The amplitude of the effect is about factor of 2 smaller than the type III 6*ω* Stark effect of WT *Rb. sphaeroides* with P oxidized (see Figure 9 in this paper). The 4*ω* Stark effect for the *β*-mutant in the B band region is so weak that it is dominated by the contribution from the intrinsic difference dipole moments of B_L and B_M. This leads to the conclusion that the driving force for $^1B_L \rightarrow B_L^+\beta_L^-$ is substantially smaller than for wild-type by at least 600 cm^{-1} from our estimate and that the rate is nearly 1 order of magnitude slower. It is interesting to note that this change in energy is considerably smaller than the in vitro change in redox potential for $BPhe/BPhe^-$ vs $BChl/BChl^-$ (300 mV or 2400 cm^{-1}).[17] There are almost no data on in situ redox potentials for modified cofactors or environmental perturbations in the B and H sites (only the P/P^+ potential can be measured directly). The results we have obtained are consistent with the shift estimated from the amplitude of delayed fluorescence measurements on the *β*-mutant which also indicated a smaller than expected energy shift in situ.[24]

It is evident that the resonance Stark effect for the *β*−mutant is very weak, and this raises the question of whether the effect is actually due to $^1B_L \rightarrow B_L^+\beta_L^-$ or possibly due to a small contribution from $^1B_M \rightarrow B_M^+H_M^-$.[25] The maximum of the B band in the *β*-mutant at 12 438 cm^{-1} (Figure 9 in part 1) is likely due to B_L absorption. Correspondingly, the larger negative peak in the 2*ω* Stark spectrum (second derivative line shape) in the B band region is also at 12 438 cm^{-1}, and this is likely due to the conventional Stark effect of B_L. On the other hand, the location of the red shoulder of the main B band can be inferred from the location of the smaller negative peak (∼12 280 cm^{-1} or 814 nm) of the 2*ω* Stark spectrum (second derivative) in the B band region, and this is likely due to B_M absorption.[26] This coincides with the location of the positive peak of the 6*ω* Stark effect in the B band region. This resonance 6*ω* Stark effect shows a band-narrowing effect, and its positive peak location should match the peak of the absorption band involved (814 nm). This suggests that the observed 6*ω* resonance Stark effect in the *β*-mutant may be due to B_M. In this case the reaction $^1B_L \rightarrow B_L^+\beta_L^-$ is even slower than the 22 ps lifetime extracted from the analysis; i.e., $(22\ ps)^{-1}$ is an upper limit for the actual rate of this reaction. If, on the other hand, the higher order Stark feature is due to $^1B_L \rightarrow B_L^+\beta_L^-$, then $(22\ ps)^{-1}$ is the upper limit for the rate of the $^1B_M \rightarrow B_M^+H_M^-$ reaction.

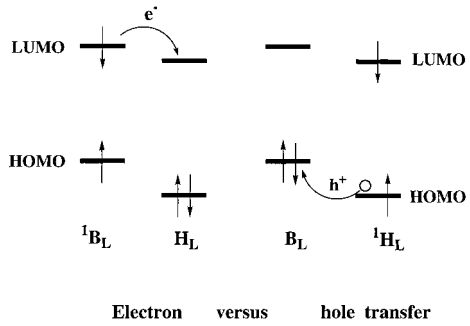

Figure 10. Schematic orbital diagram of B_L and H_L in the photosynthetic RC. The relative energy ordering between B and H in the RC is not known directly. However, it is reasonable to assume that the HOMO of H is lower than the HOMO of B because bacteriopheophytin is harder to oxidize than bacteriochlorophyll in vitro, and the LUMO of H is lower than the LUMO of B because their excitation energies are similar. As illustrated, electron transfer from ^1B to H involves coupling through their LUMOs. In contrast, hole transfer from ^1H to B involves coupling through their HOMOs.

The (M)Y210F mutant was created originally because phenylalanine is the symmetry-related residue adjacent to B_M (residue (L)178 in *Rb. sphaeroides*). On the basis of the analysis of the B band higher order Stark effect for the (M)Y210F mutant (or *C. aurantiacus*) one expects that the driving force for $^1B_M \rightarrow B_M^+H_M^-$ should be relatively large, yet there is no evidence for this process in wild-type. It appears unlikely that the electronic coupling on the M side is much different from that on the L side. At the simplest level the physical proximity of the chromophores on the L and M sides are similar, and energy-transfer experiments (see below) can be interpreted as indicating that the coupling is comparable.[27,28] This suggests that there is some compensating perturbation that makes the driving force/reorganization energy combination for $B_M^+H_M^-$ formation unfavorable. If correct, this is an interesting conclusion as most analyses of unidirectional electron transfer focus on the relative energies of ^1P and $P^+B_L^-$ vs $P^+B_M^-$. Although these experiments do not provide any further insight into the origin(s) of unidirectional electron transfer from ^1P, it is interesting that we also observe a type of unidirectionality in the comparison of $^1B_L \rightarrow B_L^+H_L^-$ vs $^1B_M \rightarrow B_M^+H_M^-$ electron transfer. It would be interesting to attempt to engineer the M side in the *β*-mutant background to favor $^1B_M \rightarrow B_M^+H_M^-$ as detected by its resonance Stark spectrum as an approach for understanding the molecular origin(s) of unidirectional electron transfer.

Implications for the Initial Electron-Transfer Step(s). The above analyses collectively support the conclusion that an interaction between ^1B_L and the $B_L^+H_L^-$ state is responsible for the resonance Stark effects in the B band region (with the possible exception of the *β*-mutant discussed above). However, other possible charge resonance interactions are possible, and it is interesting to examine these further. As illustrated on the left side of Figure 10, this means that the electron on the LUMO

of ^1B_L couples to the LUMO of H_L. It is plausible that the LUMO of H_L is lower in energy than the LUMO of B_L because BPhe has a lower reduction potential and the chromophore excitation energies are similar. We would expect that ^1H_L should also experience a weak intermolecular charge resonance interaction with B_L; yet no evidence of a resonance Stark effect was found for the H_L band (see part 1). Since the $B_L^+H_L^-$ state would be the CT state with an energy low enough to allow such interaction with ^1H_L, the interaction would be hole (right side of Figure 10) rather than electron resonance between the HOMOs of H_L and B_L. The absence of a resonance Stark effect for the H band suggests that the electronic coupling through the hole on the HOMO may not be as effective as that for the electron on the LUMO. A resonance interaction between ^1B_L and $P^+B_L^-$ could also cause a resonance Stark effect for the B band. Our data (see part 1) collectively suggest that this interaction is negligible, so it was ignored in our analysis. We can speculate on possible reasons for this. First, the energy of $P^+B_L^-$ could be higher in energy than ^1B_L. Since the ^1B_L energy is higher than ^1P, this would exclude the possibility of a two-step mechanism for electron transfer to H_L from ^1P (see below). Alternatively, since the interaction between ^1B_L and $P^+B_L^-$ involves a hole transfer between the HOMOs of B_L and P, perhaps the electronic coupling is weak for coupling through hole. The coupling between ^1P and $P^+B_L^-$ should be different because it involves coupling through electrons in the LUMOs. Finally, this latter coupling would also be expected to produce a resonance Stark effect for P, yet none is observed. The Stark effect of the special pair represents a very different physical situation,[29] and this will be discussed in detail elsewhere.[30]

There has been extensive discussion of two-step, $^1PB_LH_L \rightarrow P^+B_L^-H_L \rightarrow P^+B_LH_L^-$, vs one-step, $^1PB_LH_L \rightarrow P^+B_LH_L^-$, mechanisms for the primary electron transfer. In the one-step mechanism, B_L^- plays an essential role as a virtual intermediate enhancing the superexchange coupling between ^1P B_L H_L and P^+ B_L H_L^-. The $^1B_LH_L \rightarrow B_L^+H_L^-$ process discussed here is relevant to this discussion, especially to the second step of the two-step mechanism, because related orbitals (LUMOs) are involved in ^1B_L and B_L^-. Obviously there is the significant difference that in the second step of the two-step mechanism there is a positive charge on P (i.e., this is a charge-shift reaction), whereas $^1B_LH_L \rightarrow B_L^+H_L^-$ is a charge-separation reaction. The second step of the two-step mechanism is remarkable as it must be much faster than the first step in order for it to be difficult to detect an appreciable concentration of B_L^-. Since the first step in this mechanism is rate-limiting and occurs in about $(1.2\ ps)^{-1}$ at low temperature, the second step must be on the order of $(100\ fs)^{-1}$ for wild-type RCs. We estimate that the effective coupling for $^1B_LH_L \rightarrow B_L^+H_L^-$ is about 6 cm^{-1} (Table 3), and with $\Delta_{CT} = 1600\ cm^{-1}$, the electronic coupling V_0 for this process is about 100 cm^{-1}. A similar value should apply for $B_L^-H_L \rightarrow B_LH_L^-$. Furthermore, we find that a positive charge on P in chemically oxidized wild-type *Rb. sphaeroides* gives rise to a type III Stark effect with essentially the same coupling strength (the rate for $^1B_L \rightarrow B_L^+H_L^-$ is slowed due to reduction in the driving force as for the β-mutant). Interestingly, approximately this value has been estimated by two rather different types of electronic structure calculations.[31,32] This electronic coupling alone could support either the second step of the two-step mechanism or a one-step superexchange mechanism (if the coupling between ^1P and virtual intermediate $P^+B_L^-$ is of a comparable magnitude). However, one must take into account reorganization energy to analyze the rate of electron transfer. This problem is circumvented in our theory as we directly obtain the effective coupling strength of 6 cm^{-1} from the resonance Stark effect. This value should approximately represent the lifetime broadening due to $^1B_LH_L \rightarrow B_L^+H_L^-$, and it is not affected by the uncertainty of Δ_{CT}.

Electron vs Energy Transfer from ^1B_L. Singlet energy transfer from ^1B to P occurs very rapidly (less than 150 fs).[27,33,34] Because the electronic coupling terms that drive singlet energy transfer and electron transfer can be related when the Dexter mechanism dominates, we reasoned that measurements of ^1B_L vs ^1B_M to P singlet energy transfer could indicate whether the electronic coupling on the L side is different from that on the M side. This was accomplished by measuring the rise of ^1P spontaneous fluorescence following selective excitation of L vs M side chromophores, either by using the β-mutant, where H_M and β are spectrally well-separated at low temperature,[27] or by tuning the excitation wavelength across the H and B bands.[28] An implicit assumption of this experiment and limitation of the fluorescence upconversion method used to detect this effect is that there are no competing processes aside from energy transfer en route from ^1B to P. While this work was in progress, Van Brederode et al. suggested the involvement of charge transfer between ^1B_L and H_L for the (M)Y210W mutant.[35,36] It was suggested that electron transfer from $^1B_L \rightarrow B_L^+H_L^-$ is on the order of 100 fs in this mutant. This is comparable with the time scale for singlet energy transfer; thus in this mutant, the strategy of measuring only the ^1P fluorescence rise time would be complicated by this competing process. Although we have not yet obtained resonance Stark data for the (M)Y210W mutant,[37] it seems reasonable that it might continue the trend reported here for the (M)Y210F and *C. aurantiacus* RCs, where a type I Stark effect was observed. That is, by inserting a less polar residue in the (M)210 site (phenylalanine or leucine replacing tyrosine), B^+ is stabilized and the driving force for $^1B_L \rightarrow B_L^+H_L^-$ is increased. In the case of both wild-type and the β-mutant the rates we extract for $^1B_L \rightarrow B_L^+H_L^-$ (or $^1B_L \rightarrow B_L^+\beta_L^-$) are much slower than the singlet energy transfer rate from ^1B to P; thus, the results reported by Stanley et al.[27] should *not* be affected to any appreciable extent by this competing electron transfer from ^1B_L, and the conclusions of that work hold.

Acknowledgment. This work is supported by the Biophysics and Chemistry Programs of the National Science Foundation. We thank Professors Parson, Friesner, and Woodbury for useful comments and suggestions on this work.

Appendix

Inclusion of Liptay-Type Stark Effect. In deriving the theory for the resonance HOS effects, we ignored a possible nonzero difference dipole moment $\Delta\mu_0$ between the ground and exciton states. For example, $\Delta\mu_0 = 2.5$ D for the Q_y transition of an isolated bacteriochlorophyll monomer. A nonzero $\Delta\mu_0$ will give rise to HOS effects according to the usual Liptay theory as described in part 1 and discussed in detail elsewhere.[4,7] In the following, we consider the consequence of including this mechanism, specifically addressing the question of whether the resonance and Liptay-type HOS effects are additive.

To simplify the treatment, we first ignore the orientation average. The inclusion of $\Delta\mu_0$ causes an additional field-induced energy shift to ν_0, given as $\Delta\nu_0 = -\Delta\vec{\mu}_0\cdot\vec{F}$. The

following exact results are derived by a procedure similar to that used in deriving eq 7:

$$\Delta\epsilon(\nu, F^2) = \{\epsilon(\nu)^2\hat{\alpha}^{(2)} + \epsilon(\nu)^3\Delta\vec{\mu}^2\}\vec{F}^2 \quad (12a)$$

$$\Delta\epsilon(\nu, F^4) = \{\epsilon^2\hat{\alpha}^{(4)} + \epsilon^3[(\hat{\alpha}^{(2)})^2 + 2\hat{\alpha}^{(3)}\Delta\vec{\mu}] + \epsilon^4 3(\hat{\alpha}^{(2)}\Delta\vec{\mu}^2) + \epsilon^5\Delta\vec{\mu}^4\}\vec{F}^4 \quad (12b)$$

$$\Delta\epsilon(\nu, F^6) = \{\epsilon^2\hat{\alpha}^{(6)} + \epsilon^3[(\hat{\alpha}^{(3)})^2 + 2(\Delta\vec{\mu}\hat{\alpha}^{(5)} + \hat{\alpha}^{(2)}\hat{\alpha}^{(4)})] + \epsilon^4[(\hat{\alpha}^{(2)})^2 + 6\Delta\vec{\mu}\hat{\alpha}^{(2)}\hat{\alpha}^{(3)} + 3(\Delta\vec{\mu})^2\hat{\alpha}^{(4)}] + \epsilon^5[6(\Delta\vec{\mu}\hat{\alpha}^{(2)})^2 + 4(\Delta\vec{\mu})^3\hat{\alpha}^{(3)}] + \epsilon^6 5(\Delta\vec{\mu}^4\hat{\alpha}^{(2)}) + \epsilon^7\Delta\vec{\mu}^6\}\vec{F}^6 \quad (12c)$$

where ϵ is always a function of ν, and the complex polarizability tensors $\hat{\alpha}^{(k)}$ (k is an integer) and the complex dipole $\Delta\vec{\mu}$ are defined as shown in the right column of Table 2. Compared to eq 7, the only difference is the modification to the dipole moment term.

Under the weak charge resonance condition $\Delta_{CT}R^2 \ll \Gamma$, the most significant contribution from the resonance Stark mechanism is always the leading term ϵ^2, which has a lower order derivative (broad) line shape as all other ϵ^k ($k > 2$) terms will be much smaller. On the other hand, because the ϵ^{n+1} term is weighted by the highest power dependence of $\Delta\mu_0$, see eq 12, the contribution from the ϵ^{n+1} term will be the most significant source of the Liptay-type Stark effect if $\Delta\mu_0$ is large enough. More quantitatively, the condition $\Delta\nu_0 \gg \Delta_{CT}R^2$ must be met in order that this Liptay-type higher order derivative HOS line shape could *possibly* emerge. These two conditions can be written into a single form as: $\Gamma > \Delta\nu_0 \gg \Delta_{CT}R^2$, and when this is the case, we can ignore all the cross-terms in eq 12, while keeping only the most significant HOS effects from both the resonance Stark mechanism (ϵ^2 term) and Liptay-type Stark mechanism (ϵ^{n+1} term). After performing the orientation average, we obtained a much simpler and approximate form of eq 12

$$\Delta\epsilon(\nu, F^n) \approx \epsilon^2(\Delta_{CT}R^2)\frac{g^{(n)}}{n!}(\Delta\mu_R F)^n C_{CT}^{n\omega} + \epsilon^{n+1}(\Delta\mu_0 F)^n C_A^{n\omega}, \quad n = 2, 4, 6, \ldots \quad (13)$$

where the angle factor $C_{CT}^{n\omega}$ for resonance Stark effect is given in eq 8. If we define ζ_A as the angle between directions of intrinsic dipole $\Delta\vec{\mu}_0$ and the transition dipole moment from the ground to final state, simply changing the subscript "CT" to "A" in eq 8, one obtains the angle factor $C_A^{n\omega}$ for the Liptay-type Stark effect. From eq 13, it is seen that the resonance Stark effect (ϵ^2 term) and Liptay-type Stark effect (ϵ^{n+1} term) are parallel and *approximately* additive effects.

As discussed previously, a larger $\Delta_{CT}R^2$ term for a given absorption will also lead to narrower resonance HOS line shapes (*cf.* Figure 7). It may be necessary to distinguish whether an experimental higher order derivative-like HOS line shape is caused by a significant intrinsic dipole $\Delta\mu_0$ or by a stronger resonance interaction (larger $\Delta_{CT}R^2$). This can be achieved by measuring the angle χ dependence of HOS line shapes. Because the angle ζ_A is not necessarily the same as the angle ζ_{CT}, $C_{CT}^{n\omega}$ and $C_A^{n\omega}$ in eq 13 are often not the same. If only the resonance Stark mechanism or Liptay-type Stark mechanism applies, then the experimental HOS *line shape* does not depend on the experimental angle χ (i.e., only the *amplitude* changes); otherwise if both contribute, Liptay-type Stark effects with higher order derivative line shapes may appear with a *different* angle dependence from that of the broader resonance Stark effect. It is appealing to separate these contributions by a simple line shape subtraction method based on their different angle dependencies as suggested in eq 13. However, it must be borne in mind that eq 13 is only an approximation. These cross-terms between the resonance-induced polarizabilities and the $\Delta\mu_0$ term (see eq 12) suggest that these two sources of Stark effects are not *strictly* additive. Therefore, it would be desirable to know how good an approximate solution eq 13 is.

For the $n\omega$ Stark effect in eq 13, the amplitude ratio between the ϵ^2 term (exclusively due to resonance Stark mechanism) and the ϵ^{n+1} term (mostly Liptay-type Stark effect) is given as

$$\frac{\epsilon^2 \text{ term}}{\epsilon^{n+1} \text{ term}} \approx \frac{\epsilon^2\Delta_{CT}R^2\frac{g^{(n)}}{n!}(\Delta\mu_R)^n}{\epsilon^{n+1}(\Delta\mu_0)^n} \propto \frac{\Delta_{CT}R^2}{\Gamma}\left(\frac{\Gamma\Delta\mu_R}{\Delta\mu_0}\right)^n, \quad n = 2, 4, 6, \ldots \quad (14)$$

where the angle factors are ignored. Clearly this amplitude ratio has a much stronger dependence on the $\Gamma\Delta\mu_R/\Delta\mu_0$ term for the 6ω Stark effect than for the 2ω Stark effect because n is larger. Thus, one expects a much larger amplitude ratio between the resonance Stark effect and the Liptay-type Stark effect in the 6ω Stark spectrum than in the 2ω Stark spectrum. In particular, if the condition $\Gamma\Delta\mu_R > \Delta\mu_0$ applies, the broad resonance Stark line shape should dominate the observed 6ω Stark effect, even though the resonance Stark effect and the Liptay-type Stark effect may be of comparable magnitudes in the conventional 2ω Stark spectrum where their cross-terms likely spoil the simplicity of eq 13. Equation 13 should be a much better approximation for a higher order Stark spectrum than for the 2ω Stark spectrum. The conditions $\Gamma\Delta\mu_R F > \Delta\mu_0 F = \Delta\nu_0$ and $\Gamma > \Delta\nu_0 \gg \Delta_{CT}R^2$ can be written in a single form as Γ-$(\Delta\mu_R F) > \Delta\nu_0 \gg \Delta_{CT}R^2$, where $\Delta\mu_R F$ is dimensionless and must be less than 1 in the perturbation treatment (see eq 5).

As we have used the resonance Stark mechanism only to simulate the experimental B band higher order Stark spectra, it is important to verify that the parameters used in our calculation satisfy the condition $\Gamma(\Delta\mu_R F) > \Delta\nu_0 \gg \Delta_{CT}R^2$, under which the resonance Stark effect will dominate in a higher order Stark spectrum and use of eq 9 is justified. Γ is 110 cm^{-1}, so the $\Gamma(\Delta\mu_R F)$ term is approximately 80 cm^{-1} (Table 3). Because the difference dipole moment for the transition to the first excited (exciton) state of BChl is about 2.5 D,[4] $\Delta\nu_0$ is about 40 cm^{-1} in a 1 MV/cm electric field, which is somewhat smaller than the $\Gamma(\Delta\mu_R F)$ term. Also the $\Delta_{CT}R^2$ term is 6 cm^{-1} (see Table 3), and the condition $\Gamma(\Delta\mu_R F) > \Delta\nu_0 \gg \Delta_{CT}R^2$ is satisfied. Indeed, the resonance Stark effect increasingly dominates in a higher order Stark effect, while the Liptay-type Stark effect becomes progressively insignificant, as observed in part 1 or by the comparison in Figure 1 of this paper. Although the resonance Stark effect also contributes to the conventional 2ω Stark spectrum, the higher order Stark effect provides an advantage in the simplicity of data analysis and physical understanding. In fact, this new effect would not have been discovered were it not for the observation of anomalous, non-Liptay HOS spectra in the RC.

For both type II and III Stark effects, we did not attempt a quantitative simulation for the 2ω Stark spectra for the reasons discussed above. Nevertheless, the theory does give a qualitative understanding of the various line shapes observed for the 2ω Stark spectra. The 2ω Stark effect of type I contains a *blue*-shift line shape (see part 1), which is not observed for isolated BChl Stark effect.[4] This line shape is in fact predicted from the above theoretical calculation in Figure 5. The experimental 2ω Stark effect of type III contains a *red*-shift line shape (see

Figure 6 in part 1), again not expected for the 2ω Stark effect of isolated BChl,[4] but predicted by the above theory as shown in Figure 5. The 2ω Stark effect of type II in wild-type *Rb. sphaeroides* RC contains a band-broadening line shape (see Figure 2 in part 1), whose amplitude is larger than that of the β-mutant RC (see Figure 9 in part 1). It is plausible that part of it (Figure 2 in part 1) could be due to the resonance Stark mechanism, which predicts a band-broadening line shape as shown in Figure 5. As discussed above, a quantitative deconvolution of these two mechanisms is difficult for the 2ω Stark effect; however, a higher order Stark spectrum is increasingly dominated by the resonance Stark mechanism only. Such deconvolution is less important for a higher order Stark spectrum from which the physical parameters were readily extracted.

References and Notes

(1) Zhou, H.; Boxer, S. G. *J. Phys. Chem.* **1997**, *101*, 5759.

(2) The heterodimer special pair consists of closely associated bacteriochlorophyll and bacteriopheophytin molecules. The system considered in this work is another "heterodimer" in the sense that B_L/H_L and B_M/H_M are interacting pairs of bacteriochlorophyll and bacteriopheophytin molecules. In contrast to the heterodimer special pair, these chromophores are further apart and have a different relative geometry; consequently, their interaction is considerably weaker.

(3) Zhou, H.; Boxer, S. G. *J. Phys. Chem. B* **1998**, *102*, 9139.

(4) Lao, K.; Moore, L. J.; Zhou, H.; Boxer, S. G. *J. Phys. Chem.* **1995**, *99*, 496.

(5) Liptay, W. In *Excited states*; Lim, E. C., Ed.; Academic: New York, 1974; p 120.

(6) Lockhart, D. J.; Boxer, S. G. *Proc. Natl. Acad. Sci. U.S.A.* **1988**, *85*, 107.

(7) Boxer, S. G. In *Biophysical Techniques in Photosynthesis*; Amesz, J., Hoff, A., Eds.; Academic: Amsterdam, The Netherlands:, 1996; Vol. 3, pp 177−189.

(8) The molecular transition moment can be calculated or determined experimentally by dichroism measurements; the CT state dipole moment can be reasonably estimated from the vector connecting the centers of D^+ and A^-. Thus ζ_{CT} can be estimated from independent information.

(9) If R is not zero, it is necessary to have the sum of Γ_0 and $\pi|V_0|^2G_2(\nu)$ (at $\nu = \nu_0$), i.e., the theoretical absorption line width Γ, match the experimental absorption line width, should any comparison with experimental data be attempted.

(10) Marcus, R. A.; Sutin, N. *Biochim. Biophys. Acta* **1985**, *811*, 265.

(11) Hush, N. *Prog. Inorg. Chem.* **1967**, *8*, 391.

(12) Hopfield, J. J. *Proc. Natl. Acad. Sci. U.S.A.* **1974**, *71*, 3640.

(13) Huang, K.; Rhys, A. *Proc. R. Soc. A* **1950**, *204*, 406.

(14) Because only the relative energy between ν_0 and ν_{CT} matters, one can either change ν_0 or ν_{CT}. The latter serves as a realistic physical situation because ν_0 is often little changed.

(15) Markham, J. J. *Rev. Mod. Phys.* **1959**, *31*, 956.

(16) Ermler, U.; Fritzsch, G.; Buchanan, S. K.; Michel, H. *Structure* **1994**, *2*, 925.

(17) Fajer, J.; Brune, D. C.; Davis, M. S.; Forman, A.; Spaulding, L. D. *Proc. Natl. Acad. Sci. U.S.A.* **1975**, *72*, 4956.

(18) Middendorf, T. R.; Mazzola, L. T.; Gaul, D. F.; Schenck, C. C.; Boxer, S. G. *J. Phys. Chem.* **1991**, *95*, 10142.

(19) Nagarajan, V.; Parson, W. W.; Davis, D.; Schenck, C. C. *Biochemistry* **1993**, *32*, 12324.

(20) Parson, W. W.; Chu, Z.-T.; Warshel, A. *Biochim. Biophys. Acta* **1990**, *1017*, 251.

(21) Alden, R. G.; Parson, W. W.; Chu, Z. T.; Warshel, A. *J. Phys. Chem.* **1996**, *100*, 16761.

(22) It is important to this argument that the dipole moment of the "solvent" not be free to reorganize. In fluid polar solvents, for example, water or acetonitrile, the solvent dipole moments can reorient to stabilize either a nascent cation or anion (not necessarily to the same extent). In the case of a structured and constrained "solvent" as in a protein, this is not necessarily the case. In this case the residues are densely packed and the sample is at 77 K, so it is highly unlikely that a tyrosine residue could flip around in response to transient $B_L \rightarrow B_L^-$ formation.

(23) Jia, Y.; DiMagno, T. J.; Chan, C. K.; Wang, Z.; Popov, M. S.; Du, M.; Hanson, D. K.; Schiffer, M.; Norris, J. R.; Fleming, G. *J. Phys. Chem.* **1993**, *97*, 13180.

(24) Kirmaier, C.; Gaul, D.; Debey, R.; Holten, D.; Schenck, C. C. *Science* **1991**, *251*, 922.

(25) We note in passing that one might expect to see a resonance Stark effect for P due to coupling to B_L and H_L. At least for wild-type RCs, the intrinsic change in dipole moment, $\Delta\mu_0$, is large due to coupling with internal charge-transfer states of the special pair, and this apparently thwarts observation of the resonance Stark effect.

(26) Steffen, M. A.; Lao, K.; Boxer, S. G. *Science* **1994**, *264*, 810.

(27) Stanley, R. J.; King, B.; Boxer, S. G. *J. Phys. Chem.* **1996**, *100*, 12052.

(28) King, B. A.; Stanley, R. J.; Boxer, S. G. *J. Phys. Chem. B* **1997**, *101*, 3644.

(29) The special pair P represents a much stronger charge resonance situation within the dimer, which not just substantially broadens the P band (see ref 1), but also should determine the intradimer charge-transfer nature of the ^1P state as revealed by earlier Stark effect measurements (see: Reference 2. Hammes; et al. *Proc. Natl. Acad. Sci. U.S.A.* **1990**, 87, 5682).

(30) Moore, L. J.; Zhou, H.; Boxer, S. G. To be published.

(31) Makri, N.; Sim, E.; Makarov, D. E.; Topaler, M. *Proc. Natl. Acad. Sci. U.S.A.* **1996**, *93*, 3926.

(32) Friesner, R. *Proc. Natl. Acad. Sci. U.S.A.*, in press.

(33) Breton, J.; Martin, J.-L.; Migus, A.; Antonetti, A.; Orszag, A. *Proc. Natl. Acad. Sci. U.S.A.* **1986**, *83*, 5121.

(34) Jia, Y.; Jonas, D. M.; Joo, T.; Nagasawa, Y.; Lang, M. J.; Fleming, G. R. *J. Phys. Chem.* **1995**, *99*, 6263.

(35) Van Brederode, M. E.; Jones, M. R.; Van Grondelle, R. *Chem. Phys. Lett.* **1997**, *268*, 143.

(36) Van Brederode, M. E.; Jones, M. R.; Van Mourik, F.; Van Stokkum, I. H. M.; Van Grondelle, R. *Biochemistry* **1997**, *36*, 6855.

(37) While these papers were being reviewed, data were obtained for several new mutants. In *Rb. sphaeroides* (M)H182L a BPhe replaces B_M as in *Chloroflexux a.* RCs, but residue M210 remains Tyr. The HOS data for (M)H182L are very similar to WT, consistent with assigning the new HOS effect to B_L in WT. HOS data were obtained for (M)Y210W, analysis of which showed the energy of $B_L^+H_L^-$ is even lower in (M)Y210W than in (M)Y210F and is best described as "Type 0.5". The rate of $^1B_L \rightarrow B_L^+H_L^-$ is faster in MY210W, giving values compatible with those described in ref 36. When P is oxidized to P^+ in (M)Y210W, the HOS spectra line shapes are between those of WT and (M)Y210F ("Type 1.5"), i.e., the energy of $B_L^+H_L^-$ increases as expected. Remarkably, in the mutant (M)G203D, the HOS spectra are similar to those for (M)Y210W. Aspartic acid at position M203, near B_L, is expected to stablize B_L^+; the results indicate similar energetic consequences for (M)G203D and (M)Y210W, despite the very different amino acid changes. HOS spectra in the B-band region for heterodimer (M)H202L are similar to those for WT, suggesting that ^1B_L does not decay primarily by electron transfer. These results and others will be reported in detail elsewhere (Zhou, H.; Treynor, T.; Boxer, S. G. To be published).